第１４回数値流体力学シンポジウム
B06-4

最新渦法の注目すべき特性とラグランジュ LES 法としての課題

Attractive Features of an Advanced Vortex Method and its Subjects as a Tool of Lagrangian LES

亀本　喬司、祝　宝山、小島　成
横浜国立大学　〒240-8501　横浜市保土ヶ谷区常盤台 79-5　kame@post.me.ynu.ac.jp

Kyoji KAMEMOTO,　Baoshan ZHU and Akira OJIMA
Yokohama National University, 79-5 Tokiwadai, Hodogaya-ku, Yokohama, Japan

This paper describes the mathematical basis of an advanced vortex method of Biot-Savart law, its application results in mechanical engineering fields, development of large eddy simulation models in vortex methods and the subjects in future. It is pointed as one of the most attractive features of the vortex method that the numerical simulation using the method is considered to be a new and simple technique of large eddy simulation, because it consists of simple algorithm based on physics of flow and it provides a completely grid-free Lagrangian calculation. Typical results of numerical investigations of the unsteady flows around an airfoil oscillating in a uniform flow, complex flows through a centrifugal impeller rotating in a volute casing and others are explained.

1. Introduction

Although the recent progress of computational fluid dynamics is quite rapid, the numerical analysis of a higher Reynolds number flow seems still not so easy, from the viewpoint of engineering applications. The applicability of the conventional turbulence models of time-mean type seems questionable as far as unsteady separated flows are concerned. And the Large Eddy Simulation of Eulerian type inevitably meets crucial difficulties in its application to flows of higher Reynolds number, because the scheme essentially needs reasonably fine grids according to the magnitude of Reynolds number.

On the other hand, the vortex methods have been developed and applied for analysis of complex, unsteady and vortical flows in relation to problems in a wide range of industries, because they consist of simple algorithm based on physics of flow. Leonard (1980)[1] summarized the basic algorithm and examples of its applications. Sarpkaya (1989)[2] presented a comprehensive review of various vortex methods based on Lagrangian or mixed Lagrangian-Eulerian schemes, the Biot-Savart law or the Vortex in Cell methods. Kamemoto (1995)[3] summarized the mathematical basis of the Biot-Savart law methods.

Recently, the first International Conference on Vortex Methods has been held in 1999, in Kobe, Japan, in which a review of vortex element methods by Lewis[4], a proposal of a hybrid vortex method by Graham et al.[5], a report on vortex method analysis of turbulent flows by Bernard[6], simulation of particulate flows using a Vortex in Cell method by Walther et al.[7], a convergence study for the vortex method with boundaries by Ying[8], numerical prediction of rotor tip-vortex roll-up in axial flight by a time marching free-wake method by Lee[9], achievements and challenges by a Vortex in Cell method by Cottet[10] and other interesting works related with different kinds of vortex methods were presented. In this conference, Kamemoto and Miyasaka (1999)[11] proposed a vortex and heat elements method and showed application results of analysis of unsteady and forced-convective heat transfer around a circular cylinder in a uniform flow. After the conference, an interesting book consisting of selected papers of the conference has been published in 2000[12].

On the other hand, as well as many finite difference methods, it is a crucial point in vortex methods that the number of vortex elements should be increased when higher resolution of turbulence structures is required, and then the computational time increases rapidly. Recently, in order to overcome the crucial point, some of leading researchers examined spatial averaging models of turbulence in high Reynolds number flows for Lagrandian large eddy simulation. Leonard and Chua (1989)[13] proposed application of the Smagorinsky model in simulations of interaction between interlocked vortex rings and interaction between two colliding vortex rings. Mansfield et al. (1998)[14] (1999)[15] proposed a dynamic eddy viscosity model of subfilter-scale stresses for Lagrangian vortex element methods and applied it to simulation of collision of coaxial vortex rings. Kiya et al. (1999)[16] carried out simulation of an impulsively started round jets by a 3-d vortex method using the Smagorinsky model. Saltara et al. (1998)[17] simulated vortex shedding from an oscillating circular cylinder with use of turbulence modeling of Smagorinsky type in a Vortex in Cell method.

In this paper, attractive characteristics of the Biot-Savart law vortex methods developed and examined up to this time are described, explaining the mathematical background and showing typical results of numerical simulation of two and three-dimensional unsteady separated flows. Then, introducing the new movement of turbulence modeling for Lagrangian vortex methods, the subjects of the vortex methods which should be solved as a tool of the Lagrangian large eddy simulation are discussed.

2 Algorithms of Vortex Methods based on Biot-Savart Law

2.1 Mathematical Basis

Since the vortex methods have been developed for numerical analysis of incompressible and unsteady flow, their governing equations are thought to be based on the Navier-Stokes equation and the continuity equation for incompressible flow which are written in vector form as follows.

$$\frac{\partial \boldsymbol{u}}{\partial t}+\left(\boldsymbol{u}\cdot grad\right)\boldsymbol{u}=-\frac{1}{r}\,grad\,p+n\nabla^2\boldsymbol{u} \tag{1}$$

$$div\,\boldsymbol{u}=0 \tag{2}$$

Alternative expression of the governing equations of viscous and incompressible flow gives the vorticity transport equation and pressure Poisson equation which are derived from the rotation and divergence of Navier-Stokes equations, respectively

$$\frac{\partial \boldsymbol{w}}{\partial t}+\left(\boldsymbol{u}\cdot grad\right)\boldsymbol{w}\;=\left(\boldsymbol{w}\cdot grad\right)\boldsymbol{u}+n\nabla^2\boldsymbol{w} \tag{3}$$

$$\nabla^2 p=-r\;div(\boldsymbol{u}\cdot grad\;\boldsymbol{u}) \tag{4}$$

where $\boldsymbol{u}$ is a velocity vector. The vorticity $\boldsymbol{w}$ is defined as

$$\boldsymbol{w}\;=rot\;\boldsymbol{u} \tag{5}$$

Lagrangian expression for the vorticity transport equation (3) is given by

$$\frac{d\boldsymbol{w}}{d\;t}=\left(\boldsymbol{w}\;\cdot grad\right)\boldsymbol{u}+n\nabla^2\boldsymbol{w} \tag{6}$$

When a two-dimensional flow is dealt with, the first term of the right hand side in equation (6) disappears and so the two-dimensional vorticity transport equation is simply expressed as

$$\frac{d\boldsymbol{w}}{d\;t}=n\nabla^2\boldsymbol{w} \tag{7}$$

In the Biot-Savart law methods, the vorticity transport equation (6) is numerically solved by the operator-splitting scheme of Chorin (1973) [18]. If the vorticity of a fluid particle at time t is written as $\boldsymbol{w}\,(t)$, we obtain an approximate expression of the change of vorticity through convection and diffusion during a small time interval dt as follows.

$$\boldsymbol{w}\,(t+dt)=\boldsymbol{w}\,(t)+(\boldsymbol{w}\;\cdot grad)\boldsymbol{u}\cdot dt+n\nabla^2\boldsymbol{w}\cdot dt \tag{8}$$

In equation (8), the second term in the right hand side is based on the three-dimensional stretching of vorticity, which always becomes zero for two-dimensional flow, and the third term is the rate of viscous diffusion of vorticity. If the Reynolds number of the flow is sufficiently large, the convection term is considered much larger than the diffusion term, and thus, the third term in equation (8) may be neglected in the computation. Furthermore, if the high Reynolds number flow is two-dimensional, equation (8) is approximated by a simple equation like $\boldsymbol{w}\,(t+dt)=\boldsymbol{w}\,(t)=$ constant. Therefore, if we take a small sectional area ds for the fluid particle and the vorticity is assumed constant in this area, the two-dimensional fluid particle is thought a free vortex element which transports a constant circulation $\Gamma=\boldsymbol{w}\;ds$.

On the other hand, the motion of the fluid particle at a location $\boldsymbol{r}$ is represented by a Lagrangian form of a simple differential equation.

$$\frac{d\,\boldsymbol{r}}{d\,t}=\boldsymbol{u} \tag{9}$$

Then, the trajectory of the fluid particle over a time step dt is approximately computed from the Adams-Bashforth method as follows.

$$\boldsymbol{r}(t+dt)=\boldsymbol{r}(t)+\left\{1.5\,\boldsymbol{u}(t)-0.5\,\boldsymbol{u}(t-dt)\right\}dt \tag{10}$$

2.2 Generalized Biot-Savart Law

As explained by Wu and Thompson (1973)[32], the Biot-Savart law can be derived from integration of the vorticity definition equation (5) as

$$\begin{aligned}\boldsymbol{u}=&\int_V \boldsymbol{w}_{\,0}\times\nabla_0 G\,dv\\&+\int_S [(\boldsymbol{n_0}\cdot\boldsymbol{u_0})\cdot\nabla_0 G-(\boldsymbol{n_0}\times\boldsymbol{u_0})\times\nabla_0 G]\;ds\end{aligned} \tag{11}$$

Here, subscript “$_0$” denotes variable, differentiation and integration at a location $\boldsymbol{r}_0$, and $\boldsymbol{n}_0$ denotes the normal unit vector at a point on a boundary surface S. And G is the fundamental solution of the scalar Laplace equation with the delta function δ $(r$-$\boldsymbol{r}_0)$ in the right hand side, which is written as

$$G=\frac{1}{2p}\log\left(\frac{1}{R}\right)\qquad\text{(2-D)} \tag{12}$$

or

$$G\;=\;\frac{1}{4\,p\,R}\qquad\text{(3-D)} \tag{13}$$

here, $\boldsymbol{R}=\boldsymbol{r}-\boldsymbol{r}_0$, $R=|\boldsymbol{R}|=|\,\boldsymbol{r}-\boldsymbol{r}_0\,|$.

In equation (11), the inner product, $\boldsymbol{n}_0\cdot\boldsymbol{u}_0$ and the outer product $\boldsymbol{n}_0\times\boldsymbol{u}_0$ stand for respectively normal and tangential velocity components on the boundary surface, and they respectively correspond to source and vortex distributions on the surface.

Therefore, it is mathematically understood that a velocity field of viscous and incompressible flow is arrived at the field integration concerning vorticity distributions in the flow field and the surface integration concerning source and vortex distributions around the boundary surface as shown in Figure 1.

2.3 Calculation of Pressure

Instead of the finite difference calculation of the pressure Poisson equation represented by equation (4), the pressure in the flow field is calculated from the integration equation formulated by Uhlman (1992)[20] as follows.

$$\begin{aligned}b\;H\;+\int_S H\;\frac{\partial G}{\partial n}ds\;=&-\int_V \nabla G\,(\boldsymbol{u}\times\boldsymbol{w}\;)dv\\&-\int_S\left\{G\;\cdot\boldsymbol{n}\cdot\frac{\partial\boldsymbol{u}}{\partial t}+n\;\cdot\boldsymbol{n}\cdot(\nabla G\times\boldsymbol{w}\;)\right\}ds\end{aligned}$$

(14)

Here, β is β = 1 inside the flow and β = 1/2 on the boundary S. G is the fundamental solution given by equation (12) or (13), and H is the Bernoulli function defined as

$$H=\frac{p}{r}+\frac{u^2}{2} \tag{15}$$

here, $u=|\,\boldsymbol{u}\,|$.

2.4 Introduction of Nascent Vortex Elements

The vorticity field near the solid surface must be represented by proper distributions of vorticity layers and discrete vortex elements so as to satisfy the non-slip condition on the surface. In the advanced method developed by the group of the present authors, a thin vorticity layer with thickness h_i is considered along the body surface and the surface of outer boundary of the thin vorticity layer is discretized by a number of vortex sheet panels as shown in Figure 2.

If the flow is considered to be two-dimensional for convenience, and a linear distribution of velocity in the thin vorticity layer is assumed, the normal convective velocity V_c on a panel can be expressed using the relation of continuity of flow and the non-slip condition on the solid surface for the element of the vorticity layer [abcd] as

$$V_c = \frac{1}{s_i}\left(\frac{h_i u_i}{2} - \frac{h_{i+1}u_{i+1}}{2}\right) \tag{16}$$

here, s_i, h_i and u_i respectively denote the panel length, vorticity layer thickness and tangential velocity at a panel edge. Using the relation between the normal and tangential velocities for each panel expressed by equation (16), the strength of the vortex sheet and/or source of the panel for the following step can be calculated numerically from equation (11).

On the other hand, the vorticity of the thin shear layer diffuses through the panel into the flow field. In order to consider this vorticity diffusion, a diffusion velocity is employed in the same manner as the vorticity layer spreading method proposed by Kamemoto (1995)[3] . The vorticity layer spreading method is based on the viscous diffusion of the vorticity in the shear layer developing over a suddenly accelerated plate wall. In this case, the displacement thickness of the vorticity layer (d) diffuses with the progress of time as $d = 1.136(nT)^{1/2}$ from the solid surface at a time T. Differentiating d by T and substituting the distance of a panel from the solid surface h_i into d, we obtain the diffusion velocity V_d at the panel as follows.

$$V_d = \frac{1.136^2 v}{h_i + h_{i+1}} \tag{17}$$

here, ν is kinematic viscosity of the fluid. If the value of (V_c+V_d) becomes positive, a nascent vortex element is introduced in the flow field, where the thickness and vorticity of the element are given as follows.

$$h_{vor} = \left(V_c + V_d\right)\cdot dt \tag{18}$$

$$w_{vor} = \frac{G}{A + A_{vor}} \tag{19}$$

Here, Γ is the circulation originally involved in the element of the vorticity layer [abcd], and A and A_{vor} are the areas of the vorticity layer element and the nascent vortex element.

In case of three-dimensional flow calculation, a three-dimensional nascent vortex element of a rectangular parallelepiped is introduced in the same manner as the two-dimensional case, through each vortex sheet panel of the outer boundary of a thin vorticity layer. The details of treatments have been explained in the paper by Ojima and Kamemoto (2000)[21]. As shown in Figure 3, if a linear distribution of velocity in the thin vorticity layer is assumed, the normal convective velocity V_c on a panel can be expressed by using the relation of continuity of flow and non-slip condition on the solid surface for the element of the vorticity layer

$$V_c = \frac{1}{DS_p}\sum_{i=1}^{4}\int_{DS_i} u_{si}\,ds \tag{20}$$

here, $u_{si} = \boldsymbol{u}_i \cdot \boldsymbol{n}_{si}$ and $DS_i = h \cdot Dl_i$

Where, DS_p, $\boldsymbol{u}_i$ and $\boldsymbol{n}_{si}$ respectively denote the panel area, the velocity vector and the normal vector on the side sectional planes of the element of the vorticity layer. Using the normal velocity for each panel expressed by equation (20), the intensity of the vortex sheet and/or source of the panel for the following step can be calculated numerically from equation (11).

In the same manner as the two-dimensional case, the viscous diffusion velocity at the panel is given as

$$V_d = \frac{c^2 n}{2h}, \quad (c\text{=1.136}) \tag{21}$$

here, n is kinematic viscosity of the fluid. If V_c+V_d becomes positive, a nascent vortex element is introduced into the flow field, where the thickness and vorticity of the element are given from the relation of the vortex strength conservation as follows.

$$\boldsymbol{w}_{vor} = \frac{\int_V \boldsymbol{w}\,dv}{V + V_{vor}} \tag{22}$$

$$h_{vor} = (V_c + V_d)\cdot dt \tag{23}$$

$$V_{vor} = DS_p \cdot h_{vor} \tag{24}$$

Here, $\boldsymbol{w}$ is the vorticity originally involved in the element of the vorticity layer, V and V_{vor} are the volume of the vorticity element and the nascent vortex element. Every vortex element is introduced at the distance of $0.5h_{vor}$ from the panel as a vortex plate.

It will be noteworthy that as a linear distribution of velocity is assumed in the thin vorticity layer, the shearing stress on the wall surface is evaluated approximately from following equation as far as the thickness of the vorticity layer is sufficiently thin.

$$t_w = m\frac{\partial u}{\partial y} = -mw \tag{25}$$

2.5 Replacement with Equivalent Vortex Blobs

For simplification of numerical treatments, every nascent vortex element which is far from the solid surface, can be replaced with an equivalent discrete vortex. Either in two-dimensional or in three dimensional flow, the discrete vortex element is modelled by a vortex blob which has its own smoothed vorticity distribution and a core radius, which spreads according to the viscous diffusion expressed by the third term in the right hand side of equation (8) as explained by Kamemoto (1995)[3]. In the vortex method used by the group of the present authors, every nascent vortex element which moves beyond a boundary at the distance of four times h_i from the solid surface, is replaced with an equivalent, circular (2-D) or spherical (3-D) vortex blob of the core spreading model.

When a two-dimensional flow is dealt with, the total circulation and the sectional area of the blob core are determined to be the same as those of the rectangular nascent vortex element. As explained by Leonard (1980)[1], if a vortex blob has a core of radius ε_i and total circulation Γ_i, a

Gaussian distribution of vorticity around the center of the blob is given as

$$w(r) = \frac{G_i}{p e_i^2} \exp\left\{ -\left(\frac{r - r_i}{e_i} \right)^2 \right\} \tag{26}$$

here r_i denotes a position of the center of the blob. As explained by Kamemoto (1995) [3], the spreading of the core radius ε_i according to the viscous diffusion expressed by equation (7) is represented as

$$\frac{de_i}{dt} = \frac{2.242^2 v}{2e_i} \tag{27}$$

When a three-dimensional flow is treated, a nascent vortex element of a rectangular parallelepiped is replaced by an equivalent vortex blob with a spherically symmetric distribution of vorticity which was proposed by Winckelmans and Leonard (1988) [22] and modified by Nakanishi and Kamemoto (1992)[23]. The details of treatments are explained in the paper by Ojima and Kamemoto (2000)[21]. A vortex blob is a spherical model with a radially symmetric distribution of vorticity. Once the *i-th* vortex blob is given in a flow field by the position $\boldsymbol{r}_i=(r_x, r_y, r_z)$, its vorticity $\boldsymbol{w}_i=(w_x, w_y, w_z)$ and its core radius e_i, the vorticity distribution around the vortex blob is represented by following equations.

$$\boldsymbol{w}_i(\boldsymbol{r}) = \boldsymbol{w}_i \ p(|\boldsymbol{r} - \boldsymbol{r}_i| / e_i) e_i^{-3} dv_i \tag{28}$$

$$p(x) = 15/8p \ (x^2 + 1)^{-7/2} \tag{29}$$

Here, $p(x)$ is smoothing function proposed by Winckelmans & Leonard (1988) [6]

On the other hand, the evolution of vorticity is calculated by equation (8) with three-dimensional core spreading method modified by Nakanishi & Kamemoto (1992)[23]. In this method, the stretch term and diffusion term of equation (8) are separately considered. The change of core radius due to the stretching is calculated from following equations.

$$\frac{d\boldsymbol{w}}{dt} = (\boldsymbol{w} \cdot grad)\,\boldsymbol{u} \tag{30}$$

$$\frac{dl}{dt} = \frac{l_t}{|\boldsymbol{w}_t|} \cdot \left| \frac{d\boldsymbol{w}}{dt} \right| \tag{31}$$

$$\left(\frac{de}{dt} \right)_{stretch} = -\frac{e_t}{2 \cdot l_t} \frac{dl}{dt} \tag{32}$$

Here, *e* and *l* are the core radius and the length of the vortex blob model as shown in Figure 4. The viscous term of equation (8) is expressed by the core spreading method. The core spreading method is based on the Navier-Stokes equation for viscous diffusion of an isolated two-dimensional vortex filament in a rest fluid, and as well as equation (27), the rate of core spreading is represented as follows.

$$\left(\frac{de}{dt} \right)_{diffusion} = \frac{c^2 n}{2e_t}, \qquad (c=2.242) \tag{33}$$

Taking account of two factors expressed as equations (32) and (33), characteristic values of the elongated blob element are obtained from the following equations.

$$e_{t+Dt} = e_t + \left[\left(\frac{de}{dt} \right)_{stretch} + \left(\frac{de}{dt} \right)_{diffusion} \right] \cdot Dt \tag{34}$$

$$l_{t+Dt} = l_t + \frac{dl}{dt} \cdot Dt \tag{35}$$

$$|\boldsymbol{w}_{t+Dt}| = |\boldsymbol{w}_t| \cdot \left(\frac{e_{t+Dt}}{e_t} \right)^2 \tag{36}$$

And then,, the elongated element is replaced into a new and spherical vortex blob which has the volume equivalent to the elongated one.

2.6 Numerical Procedure.

If all of the vorticity layers existing in the flow field at any time are represented with discrete vortex distributions, the strengths of the source and/or vortex distributed along the boundary surface are numerically calculated so as to satisfy the boundary conditions of normal or tangential velocity components on it, by applying the popular scheme of the panel method to the integration equation (11). Once the source and/or vortex distributions are determined in the right hand side of equation (11), not only a flow velocity at an arbitrary position in the flow field but also the convective velocity of each discrete vortex can be calculated. Substituting the velocities into equations (8) and (10), the vorticity transport and trajectory of each discrete vortex over the time step are numerically investigated, which provide new distributions of discrete vortices corresponding to the vorticity layers transported during the time step.

Consequently, the iteration of the above procedure provides the basic scheme of the grid-free Lagrangian simulation of unsteady, incompressible and viscous flow, making use of the Biot-Savart law vortex methods.

2.7 Application to Forced Convective Heat Transfer

When a forced heat convection in a flow of a high Reynolds number and a not-so-small Prandtl number is assumed, we can ignore the effects of natural heat convection. Then, the energy equation for forced convective heat transfer is expressed as

$$\frac{\partial T}{\partial t} + (\boldsymbol{u} \cdot grad)\,T = a \nabla^2 T \tag{37}$$

where T is temperature and α is the thermal diffusivity. Lagrangian expression for the energy equation (37) are given by

$$\frac{dT}{dt} = a \nabla^2 T \tag{38}$$

It is clear that the energy equation (38) is of the similar form to the vorticity transport equation (6). When a two-dimensional flow is dealt with, the vorticity transport equation is simply expressed by equation (7). Therefore, the form of equation (38) becomes completely the same as equation (7). This fact seems to suggest that the energy equation (38) can be solved in an analogous way, with nascent temperature elements, in place of vortex elements using a time splitting scheme.

In the vortex element method developed by the group of the present authors, the viscous diffusion expressed by equation (7) is approximately taken into account by the core spreading method. Therefore, in the present method, the thermal diffusion expressed by equation (38) is similarly considered by introducing a thermal core to a discrete heat element which spreads with the increase of time, and as same as that of a vortex element, the trajectory of each heat element in flow is represented by equation (9).

The details of teatments in the calculation of forced convective heat transfer are explained in the paper by Kamemoto and Miyasaka (1999)[11].

3 The Way to Lagrangian Large Eddy Simulation

3.1 Turbulence Models for the Vortex Methods

When treating high Reynolds number flows, one can perform a large eddy simulation by modeling the effect of the small or subgrid-scale eddies on the larger scales. In their study on three-dimensional interactions of vortex tubes, Leonard and Chua (1989)[13] proposed and used a nonlinear core-spreading algorithm, which is a pioneering work of modeling turbulence for a vortex method in the spirit of large eddy simulation. To accomplish this in a vortex method, they introduced a subgrid-scale viscosity n_{SGS} and implemented the following nonlinear core-spreading algorithm for expression of changing rate of core radius e_i,

$$\frac{de_i^2}{dt} = 4n_{SGS} - e_i^2 \frac{1}{w}\frac{dw}{dt} \tag{39}$$

where $w = |\boldsymbol{w}|$, and the second term on the right-hand side is the inviscid change in core size due to stretching of vorticity and the subgrid-scale viscosity depends on the local vorticity stretching rate $(1/w)$ (dw / dt), as follows.

$$n_{SGS} = \max\left[0, Ce_i^2 \frac{1}{w}\frac{dw}{dt}\right] \tag{40}$$

where C is a constant. They have pointed out that the expression (40) for $_{SGS}$ is very similar in form to the so-called Smagorinsky model used in large eddy simulation with finite difference methods and given by

$$n_{SGS} = C'D^2 \left(\frac{\partial u_i}{\partial x_k}\frac{\partial u_k}{\partial x_i}\right)^{1/2} \tag{41}$$

where C' is a constant and D is the scale of grid. Using the nonlinear core-spreading scheme in simulations of interaction between two interlocked vortex rings and interaction between two colliding vortex rings, Leonard and Chua succeeded in observing the dynamics of the space curves of the vortex tubes, the development of complex internal structure in the vortex cores and the reconnection of vortex lines.

Mansfield et al. (1998)[14] (1999) [15] developed a dynamic eddy viscosity model of the subfilter-scale stresses for Lagrangian vortex element methods. Their LES scheme is based on the filtered vorticity transport equation which is expressed as

$$\frac{\partial \bar{\boldsymbol{w}}_i}{\partial t} + \bar{\boldsymbol{u}}_j \frac{\partial \bar{\boldsymbol{w}}_i}{\partial x_j} = \bar{\boldsymbol{w}}_j \frac{\partial \bar{\boldsymbol{u}}_i}{\partial x_j} + n\nabla^2 \bar{\boldsymbol{w}}_i - \frac{\partial \boldsymbol{R}_{ij}}{\partial x_j} \tag{42}$$

In this equation, $\boldsymbol{R}_{ij}$ is the subfilter-scale (SFS) vorticity stress, which accounts for the effect of unresolved velocity and vorticity fluctuations and is expressed as

$$\boldsymbol{R}_{ij} \equiv \left(\overline{\boldsymbol{w}_i \boldsymbol{u}_j} - \bar{\boldsymbol{w}}_i \bar{\boldsymbol{u}}_j\right) - \left(\overline{\boldsymbol{u}_i \boldsymbol{w}_j} - \bar{\boldsymbol{u}}_i \bar{\boldsymbol{w}}_j\right) \tag{43}$$

where bars are used to denote spatially filtered quantities. In order to close the filtered vorticity transport equation (42), they provided a model for the vorticity stress $\boldsymbol{R}$ based on the eddy diffusivity model

$$\nabla\cdot\boldsymbol{R} = -\nabla\cdot\left(n_T \nabla\bar{\boldsymbol{w}}\right) \tag{44}$$

where the eddy diffusivity is expressed as

$$n_T = C_r^2 D^2 |S| \tag{45}$$

here, the modulus of the filtered strain-rate tensor is defined as $|S| = (2S_{mn}S_{mn})^{1/2}$. In equation (45), D is the filter size which is related to the core size of the vortex elements used to represent the vorticity field, and C_r is a model constant which is determined locally in the calculations according to filtering operations. Applying the LES model to simulation of the collision of coaxial vortex rings, Mansfield et al (1999)[29] showed that the Lagrangian LES scheme captures several experimentally observed features of the ring collisions, including turbulent breakdown into small-scale structures and the generation of small-scale radially propagating vortex rings.

Recently, Kiya et al (1999) [16] modified the nonlinear core-spreading algorithm proposed by Leonard and Chua and examined the effect of the subgrid-scale eddies on the flow of larger scales. In the original model of Leonard and Chua, as shown in equation (40), if $dw/dt<0$, the subgrid-scale viscosity n_{SGS} becomes $n_{SGS} = 0$. Kiya et al., however, did not use this procedure, but they simply applied the sub-grid scale viscosity based on the Smagorinsky sub-grid scale viscosity, which is expressed as

$$n_{SGS} = c^2 D^2 \frac{1}{w}\frac{dw}{dt} \tag{46}$$

where D is replaced by the core radius e_i of a vortex element and the value of the model constant $c = 0.17$, which is recommended for free turbulent shear flows in the Smagorinsky model, was employed in their study. They examined three models of core spreading based on viscous diffusion, turbulent eddies and both effects, which are respectively expressed as

$$\frac{de_i^2}{dt} = 4n \tag{47}$$

$$\frac{de_i^2}{dt} = 4n_{SGS} \tag{48}$$

$$\frac{de_i^2}{dt} = 4\left(n + n_{SGS}\right) \tag{49}$$

Applying each models to an impulsively started round jet forced by two helical disturbance rotating in the counter directions, Kiya et al. compared vortical structures in the jet among the models, and concluded that the simulation of the forced round jet by the turbulence model seems to generate turbulent vortical structures although its validation based on DNS or experiments is left as a study in the future.

3.2 On Challenge to Modeling of Wall Turbulence.

So far, all of the turbulence models described above have been applied only for free turbulence. Saltara et al. (1998)[17] simulated vortex shedding from an oscillating circular cylinder with use of turbulence modeling in a vortex in cell method. However, any challenging works on modeling of wall turbulence for the Lagrangian vortex methods have not been reported, yet.

As the algorithms of the advanced vortex method explained in the section 2 are very simple, it seems not so difficult to take account of the effects of subcore (subfilter) eddies on the flow represented with discrete vortices. Therefore, it will be very interesting to test the SGS models proposed for free turbulence in simulation of a high Reynolds number flow around a bluff body.

4 Application Examples

For investigation of unsteady and vortical flows, the Biot-Savart law vortex methods have so attractive advantages that grid generation in a flow field is not necessary and any conventional turbulence models of time-mean type are not used. Therefore, the vortex methods have been applied for analyses of unsteady separated flows related with various problems in engineering fields. The followings are typical examples of application of the advanced vortex method by the group of the present author.

4.1 Unsteady Flow past an Oscillating Airfoil

In order to examine the effectiveness of the present method, the two-dimensional unsteady separated flow past a sinusoidally oscillating NACA 0012 airfoil was computed by Etoh et al. (1997) [24]. Figure 5 shows instantaneous flow patterns at the mean angle of attack a = 15.0^o during pitching up and down motion, when the airfoil was oscillated in pitch angle about the quarter chord point as a = 15.0^o +5.0 sin $W T$ at the Reynolds number Re=5.0 × 10^5, where T is the non-dimensional time based on the cord length and the velocity of uniform flow, and the non-dimensional time step was dT=0.026 and W was given as W=1.0. It is clearly shown that in the case of pitching down motion, the large dynamic stall vortex and trailing edge vortex still exit around the airfoil, whereas in the case of pitching up motion, the dynamic stall is developing but the both vortices are not so large, yet.

4.2 Unsteady Flows around Three-dimensional Bluff Bodies

Recently, in order to confirm the applicability of an advanced vortex method to a three-dimensional unsteady separated flow, the developments of vortical wakes behind a sphere and a prolate spheroid after their impulsive start at a constant speed in a rest fluid were simulated by Ojima and Kamemoto (2000) [21]. In their calculation, both a sphere and the prolate spheroid were represented by 360 source and vortex panels.

Figure 6 shows calculated instantaneous flow patterns represented by discrete vortices and isosurfaces of streamwise vorticity behind the sphere at a non-dimensional time tU/D=10.25 elapsed after the start at a Reynolds number Re=300, where U and D denote the speed and the diameter of the sphere respectively, and the time step size was dtU/D =0.05. In this figure, three-dimensional vortex structures are clearly shown in the separated flow, and the development of spiral structure of wake and the interesting phenomenon like the break-down of hear pin vortices into turbulence vortices of small scale can be observed in the wake.

Figure 7 shows instantaneous flow patterns behind the prolate spheroid of the axis ratio b/a=1/3 represented by discrete vortices and isosurface of the streamwise vorticity for tU/D=10.25, attack-angle a=0.0^o and Re=Ua/n=1,000, where a and b denote the length of major and minor axes respectively, and the time step size was dtU/D =0.075. It is seen that the typical hairpin-shaped structure begins to be periodically formed behind the spheroid in the similar manner to the wake of a sphere as shown in Figure 6.

4.3 Unsteady Flow in a Centrifugal Pump

The advanced vortex method has been applied to such an engineering purpose as simulation of unsteady and complex flow through a two-dimensional centrifugal impeller by Zhu et al. (1998)[25]. Figure 8 shows an instantaneous pattern of flow through the impeller in the case of partial discharge (60% of the design flow rate) at a non-dimensional time T=2.0 after the start of rotation at a constant speed at the Reynolds number Re=10^5, where the time step size was dT=0.01 and the non-dimensional value were based on the inlet meridian velocity at the design condition and the outer diameter of the impeller. It is clearly demonstrated that the flow becomes completely non-axi-symmetrical and some of blade-to-blade passages seem to be blocked with separation bubbles.

4.4 Rotor-Stator Interaction in a Diffuser Pump

As the flow-unsteadiness generated by rotor-stator interaction in turbomachinery usually causes serious problems concerning vibration and noise, development of easy-to-handle methods have been expected to simulate the real unsteady-interaction without introducing either a sliding-surface between the rotating and stationary frames or turbulence models of time-mean type. In order to examine the applicability of the advanced vortex method for those purposes, the unsteady and interactive flows between a two-dimensional centrifugal impeller and a surrounding vaned diffuser were simulated by Zhu and Kamemoto (1999)[26]. In the calculation, each vane of the impeller and diffuser was represented 50 vortex panels, and the time step size and Reynolds number were taken as dt=T/150 and Re=10^5 respectively, here T is the period of impeller revolution. Figure 9 shows examples of calculated instantaneous pressure distribution at a time and variation of static pressure with time at a point close to the suction-side of leading edge of a diffuser vane compared with experimental data. [29]. It is found that there exist considerable differences of static pressure in the flow field around the diffuser inlet corresponding to the relative position between impeller and diffuser vanes. And it is one of the most interesting points that variation of the calculated pressure coefficient Cp is in very good agreement with experimental one in its absolute value.

4.5 Simulation of Three-dimensional Unsteady Flows through a Wind Turbine

In relation with further development of promising clean energy resources, investigations of unsteady and three-dimensional characteristics of flows around wind turbines are required. Especially, for conditions out of the conventional design, it is necessary to predict the features of complex vortical flows to design suitable operation procedures. Corresponding to those requirements, simulation of three-dimensional and unsteady flows through a horizontal-axis wind turbine (HAWT) of single blade was performed applying the advanced vortex method by Ojima and Kamemoto (2000)[27]. In the calculation, the blade was divided into 572 source and vortex panels (span wise: 22, sectional blade element: 26), and the time step size and Reynolds number were taken as $dtV/R=2\pi/(200\Omega)$ and $Re=VR/\nu=1.0\times10^6$, where V, R and Ω denote the blade tip velocity, the rotational radius of the blade tip and angular velocity. Figure 10 shows calculated instantaneous flow pattern represented by discrete vortices at tip speed ratio $\lambda=V/U=8.0$ after three times of rotor revolution, where U is a wind velocity. At the initial stage of the flow, complex wake structure is formed behind the rotor blade due to interaction among starting vortices shed from the trailing edge and the longitudinal vorticesshed from the tip and root of the blade. And it is observed that as time goes on, the starting vortices flow downstream and the longitudinal vortices tend to have dominant role in the flow field. Figure 11 shows instantaneous pressure distributions on the blade surfaces after three rotor revolutions for $\lambda=8.0$. It is seen that a lower pressure region develops near the tip and leading edges on the suction side of the blade.

4.6 Numerical Fish

Recently, in relation to conservation of fish resources, development of numerical prediction technique for confirmation of safe swimming of fishes through a hydraulic turbine of a power station. For this purpose, the group of the present authors[28] have started to apply their vortex methods to numerical simulation of fish swimming. Figure 12 (a) shows shows the aspect of swimming of a two-dimensional trout obtained from a 2-D calculation. Blue vortex elements means clockwise rotation and red elements are counter-clockwise vortices. We can find that there is no separation region around the fish and alternative vortex rows are formed behind the fish. Figure 12 (b) shows the instantaneous presuure distribution on the skin of a trout obtained from 3-D calculation, here, the red skin shows a higher pressure region and blue one is a lower pressure region.

5 Conclusions

In this paper, the mathematical basis of the methods, calculation algorithms and an advanced vortex method developed by the group of the present author were explained in the section 2.

In the section 3, recent pioneering works on LES modeling by leading researchers were reviewed, and necessity of development of wall turbulence models was described

In the section 4, from the various examples of application, it was confirmed that the vortex methods standing on the Biot-Savart law are consisting of simple algorithms based on physics of flow and they provide completely grid-free Lagrangian calculation.

Finally, it may be possible to say that the advanced vortex methods are to yield a promising way to a grid-free Lagrangian Large Eddy Simulation of unsteady and complex flows of higher Reynolds numbers.

References

[1] Leonard, A., : Vortex methods for flow simulations, J. Comp. Phys. 37, (1980), pp. 289-335.

[2] Sarpkaya, T. : Computational methods with vortices - the 1988 Freeman scholar lecture, J. Fluids Engng., 111, (1989), pp.5-52.

[3] Kamemoto, K. : On attractive features of the vortex methods, Computational Fluid Dynamics Review 1995, ed. M.Hafez and K.Oshima, JOHN WILEY ¥& SONS, (1995), pp.334-353.

[4] Lewis R.I. : Vortex element methods, the most natural approach to flow simulation - a review of methodology with applications, Proc. of 1st Int. Conf. on Vortex Methods, Kobe, Nov.4-5, (1999), pp.1-15.

[5] Graham J.M.R. and Arkell R.H. : A hybrid vortex method, Proc. of 1st Int. Conf. on Vortex Methods, Kobe, Nov.4-5, (1999), pp.47-58.

[6] Bernard P.S., Dimas A.A. and Lottati I. : Vortex method analysis of turbulent flow, Proc. of 1st Int. Conf. on Vortex Methods, Kobe, Nov.4-5, (1999), pp.137-155.

[7] Walther J.H. and Sagredo J.T. and Koumoutsakos P. : Simulation of particulate flow using vortex methods, Proc. of 1st Int. Conf. on Vortex Methods, Kobe, Nov.4-5, (1999), pp.221-231.

[8] Ying L. : Convergence study for the vortex method with boundaries, Proc. of 1st Int. Conf. on Vortex Methods, Kobe, Nov. 4-5, (1999), pp.235-242.

[9] Lee D. : Numerical prediction of rotor tip-vortex roll-up in axial flight by using a time-marching free-wake method, Proc. of 1st Int. Conf. on Vortex Methods, Kobe, Nov.4-5, (1999), pp.243-253.

[10] Cottet G.H. : 3D vortex methods: achievements and challenges, Proc. of 1st Int. Conf. on Vortex Methods, Kobe, Nov.4-5, (1999), pp.315-329.

[11] Kamemoto K. and Miyasaka T. : Development of a vortex and heat elements method and its application to analysis of unsteady heat transfer around a circular cylinder in a uniform flow, Proc. of 1st Int. Conf. on Vortex Methods, Kobe, Nov.4-5, (1999), pp.191-203, or VORTEX METHODS, edited by K. Kamemoto & M. Tsutahara, *World Scientific*, (2000), pp.135-144.

[12] VORTEX METHODS, edited by K. Kamemoto & M. Tsutahara, *World Scientific*, (2000).

[13] Leonard A. and Chua K. : Three-dimensional interaction of vortex tubes, Pysica D (Nonlinear Phenomena), 37, (1989), pp.490-496.

[14] Mansfield J.R., Knio O.M. and Meneveau C. : A dynamic LES scheme for the vorticity transport equation :Formulation and a priori tests, J. of Comp. Phys., 145, (1998), pp.693-730.

[15] Mansfield J.R., Knio O.M. and Meneveau C. : Dynamic LES of colliding vortex rings using a 3D vortex method, J. of Comp. Phys., 152, (1999), pp.305-345.

[16] Kiya M., Izawa S. and Ishikawa H. : Vortex method simulation of forced, impulsively started round jet, Proc. of the 3rd ASME/JSME Joint Fluids Engng. Conf. San Francisco, July 18-22, (1999), FEDSM99-6813.

[17] Saltara F., Meneghini J.R., Siqueira C.R. and Bearman P.W. : The simulation of vortex shedding from an oscillating circular cylinder with turbulence modelling, 1998 ASME FEDSM, Proc. of 1998 Conf. on Bluff Body Wakes and Vortex-Induced Vibration, (1998), Paper No. 13.

[18] Chorin, A.J. : Numerical study of slightly viscous flow, J. Fluid

Mech. 57, (1973), pp.785-796.

[19] Wu, J.C. and Thompson, J.E., : Numerical solutions of time-dependent incompressible Navier-Stokes Equations using an integro-differential formulation. Computers & Fluids 1, (1973), pp.197-215.

[20] Uhlman, J.S., : An integral equation formulation of the equation of motion of an incompressible fluid. Naval Undersea Warfare Center T.R. 10-086. (1992).

[21] Ojima A. and Kamemoto K. : Numerical simulation of unsteady flow around three dimensional bluff bodies by an advanced vortex method, JSME Int. Journal, B, 43-2, (2000), pp.127-135.

[22] Winkelmans, G. and Leonard, A. : Improved vortex methods for three-dimensional flows, Proc. Workshop on Mathematical Aspects of Vortex Dynamics. 25-35. (1988), Leeburg. Virginia.

[23] Nakanishi, Y. and Kamemoto, K. : Numerical simulation of flow around a sphere with vortex blobs, J. Wind Engng and Ind. Aero., 46 and 47, (1992), pp.363-369.

[24] Etoh, F., Kamemoto, K., Matsumoto, H. and Yokoi, Y. : Numerical simulation of flow around a rotary oscillating foil with constant amplitude angle by use of the vortex method, Proc. 11th Symp. on CFD, Tokyo, (1997), pp.385-386. Chorin, A.J. : Vortex sheet approximation of boundary layers. J. Comp. Phys. 74, (1978), pp.283-317.

[25] Zhu, B., Kamemoto, K. and Matsumoto, H., Computation of unsteady viscous flow through centrifugal impeller rotating in volute casing by direct vortex method, Comp. Fluid Dynamics J. 7-3, (1998), pp.313-323.

[26] Zhu, B. and Kamemoto, K., : Simulation of the unsteady interaction of a centrifugal impeller with its diffuser by an advanced vortex method. Proc. of the 3rd ASME/JSME Joint Fluids Engng. Conf. San Francisco, July 18-22, (1999), FEDSM99-6821.

[27] Ojima A. and Kamemoto K. : Numerical simulation of unsteady flow around three-dimensional blades of a wind turbine by a vortex method, Proc. of 2000 ASME FEDSM, Boston, (2000), FEDSM2000-11078.

[28] Iso, Y. ; Study on development of numerical fish, Master Thesis at Department of Mechanical Engineering,, Yokohama National University , (2000-3).

[29] Tsukamoto H., Uno M., Hamafuku H. and Okamura T. : Pressure fluctuation downstream of a diffuser pump impeller. Proc. of 2nd Joint ASME/JSME Fluid Engng. Conf., FED-vol. 216, (1995), pp.133.

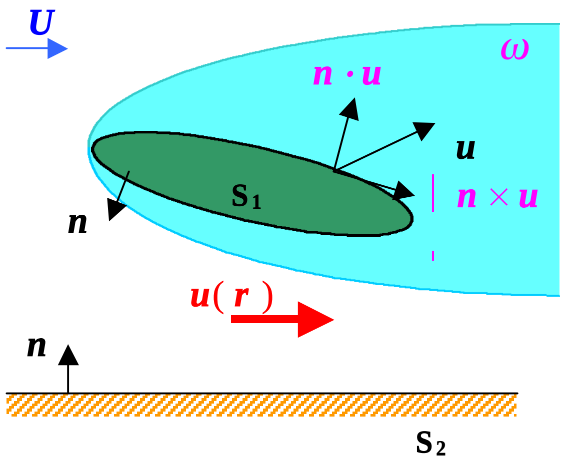

Figure 1: Flow field involving vorticity region.

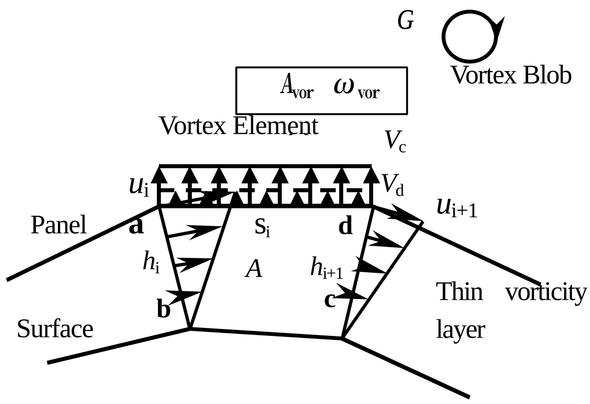

Figure 2: Thin vorticity layer and nascent vortex element

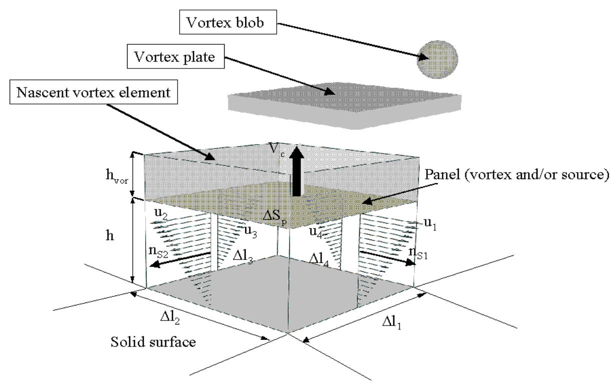

Figure 3: Introduction of three-dimensional nascent vortex element.

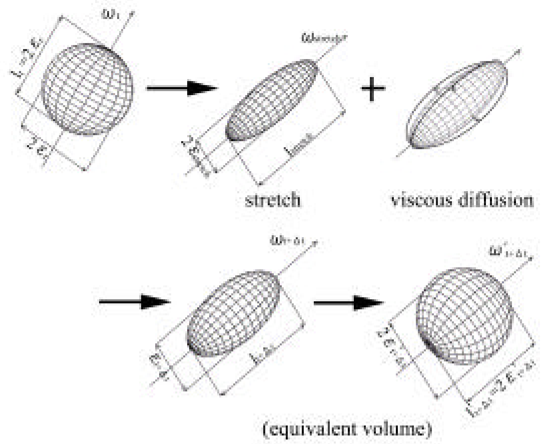

Figure 4: Mechanism of three-dimensional core spreading method for a vortex blob.

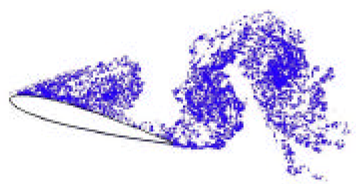

(a) Pitching down at $a = 15.0^{o}$ ($T = 11.0$)

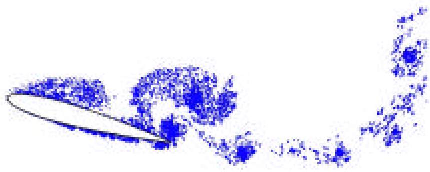

(b) Pitching up at $a = 15.0^{o}$ ($T = 14.1$)

Figure5: Instantaneous flow patterns around an oscillating airfoil NACA 0012 .($a = 15.0^{o} + 5.0 \sin W T$, $Re = 5.0 \times 10^{5}$)

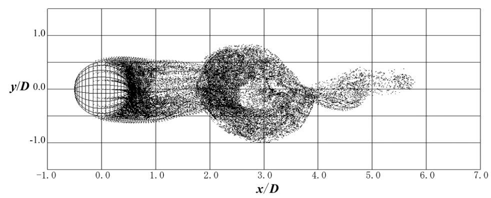

(a) Flow pattern.

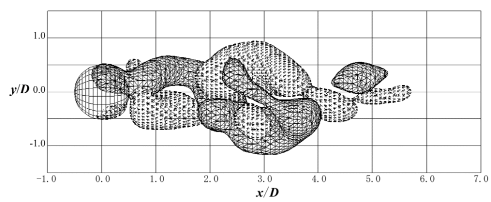

(b) Isosurfaces of streamwise vorticity.

Figure6: Instantaneous flow patterns represented by discrete vortices and isosurfaces of streamwise vorticity behind a sphere (*tU/D*=10.25, *Re*=300).

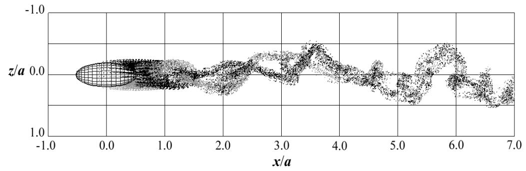

(a) Flow pattern.

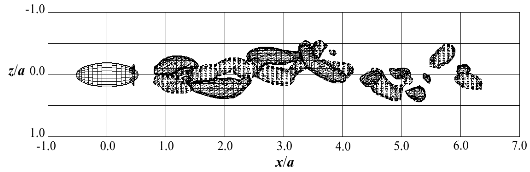

(b) Isosurfaces of streamwise vorticity.

Figure 7: Instantaneous flow patterns represented by discrete vortices and isosurfaces of streamwise vorticity behind a prolate spheroid (*tU/D*=10.25, a=0.0^{o}, *Re*=1,000).

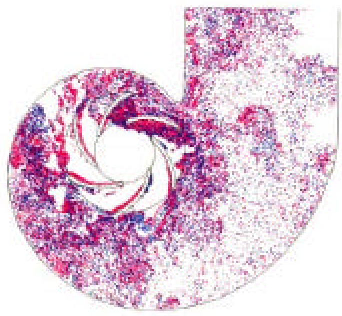

(a) Flow pattern represented by discrete vortices.
(b)

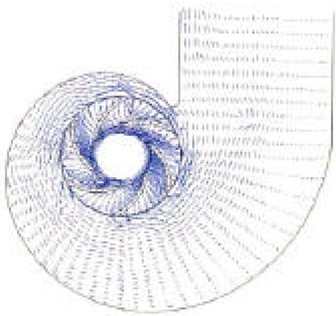

(b) Velocity vectors.

Figure 8: Two-dimensional unsteady flow in a centrifugal pump at 60% of the design flow rate.

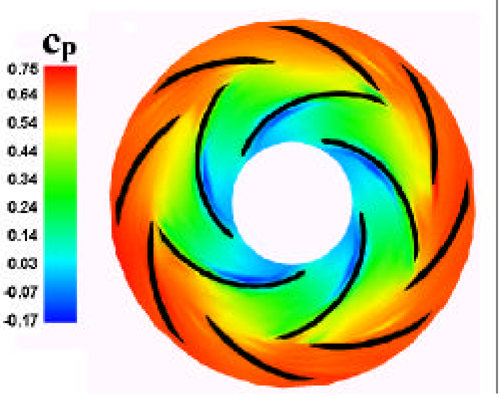

(a) Instantaneous pressure distribution

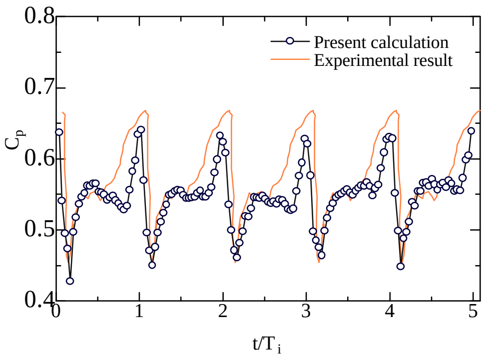

(b) Variation of static pressure with time at a point close to the suction-side of leading edge of a diffuser vane

Figure 9: Interactive pressure distribution around rotor and stator vanes in a diffuser pump (100%).

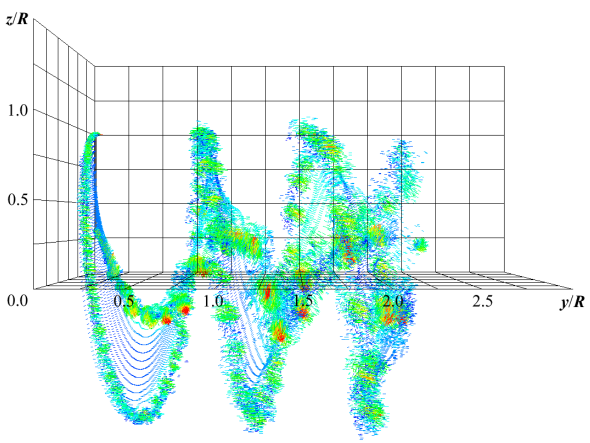

Figure10: Instantaneous flow pattern behind a wind turbine after three times of rotor revolution at tip speed ratio λ=8.0

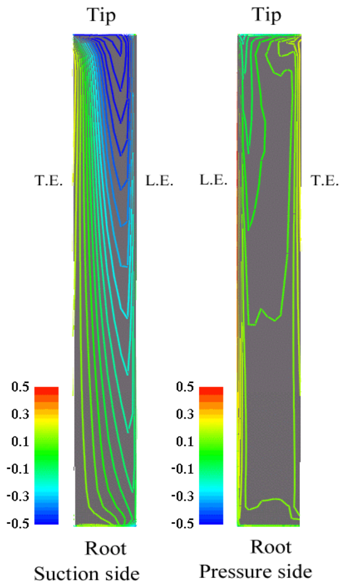

Figure 11: Instantaneous pressure distributions on the blade surfaces after three rotor revolutions for λ=8.0

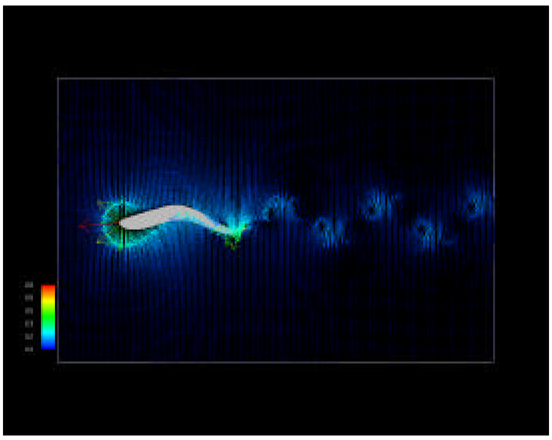

(a) Flow around a swimming trout (2-D).

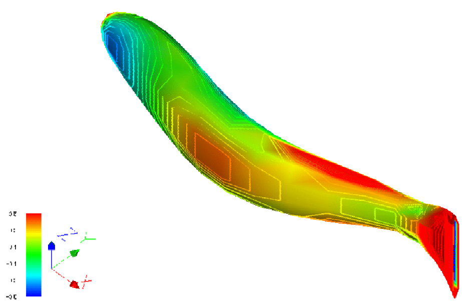

(b) Instantaneous pressure distribution around a trout (3-D).

Figure 12: Flow around a numerical fish.